Electronic structures of finite double-walled carbon nanotubes in a magnetic field



2008 J. Phys.: Condens. Matter 20 075213

(http://iopscience.iop.org/0953-8984/20/7/075213)

J. Phys.: Condens. Matter **20** (2008) 075213 (8pp) doi:10.1088/0953-8984/20/7/075213

# Electronic structures of finite double-walled carbon nanotubes in a magnetic field

**C H Lee[1], Y C Hsue[1], R B Chen[2], T S Li[3] and M F Lin[1]**

[1] Department of Physics, National Cheng Kung University, Tainan, Taiwan, Republic of China
[2] Center for General Education, National Kaohsiung Marine University, Kaohsiung 830, Taiwan, Republic of China
[3] Department of Electrical Engineering, Kun Shan University, Tainan, Taiwan, Republic of China

Received 10 August 2007, in final form 11 December 2007
Published 28 January 2008
Online at stacks.iop.org/JPhysCM/20/075213

**Abstract**

The discrete electronic states of finite double-walled armchair carbon nanotubes are obtained in a magnetic field by using the Peierls tight-binding model. State energy, wavefunction, energy gap, and density of states are investigated in detail. Electronic properties strongly depend on the intertube atomic interactions, magnitude and direction of the magnetic field, boundary structure, length, and Zeeman splitting. The intertube atomic interactions result in an asymmetric energy spectrum about the Fermi level, a drastic change in energy gap, and obvious energy shifts. The magnetic field could lead to state crossing, alter the hybridization of the inner and outer tight-binding functions, destroy state degeneracy, increase more low-energy states, and induce complete energy-gap modulations (CEGMs). The different atomic positions along the tube axis make the $C_5$ system differ from the $D_{5h}$ or $S_5$ systems. According to the lengths $N_l = 3i, 3i + 1$, and $3i + 2$ ($i$ an integer), there exist three types of magnetic-flux-dependent state energies. The Zeeman effect causes CEGMs to happen at weaker magnetic fields. The main features of quantized electronic states are directly reflected in the density of states. The predicted magneto-electronic properties could be examined by the transport and optical measurements.

## 1. Introduction

After carbon nanotubes (CNs) were discovered in 1991 by Iijima [1] they attracted a lot of attention owing to their unique electronic properties. A single-walled CN (SWCN) is a quasi-one-dimensional (Q1D) system, and it can be regarded as a rolled-up 2D graphite sheet in cylindrical form. Furthermore, a zero-dimensional (0D) finite CN is fabricated by cutting a long CN into segments [2]. The main difference between a Q1D nanowire and a 0D quantum dot lies in the many quantized discrete states of the latter. The electronic states are discretized due to the finite length. The quantum-size effect has been verified by experimental measurements of transport properties [3–8]. For theoretical studies on 0D CNs, first-principles calculations and the tight-binding model are used to investigate electronic structures [9–15], magnetic properties [12–15], and optical excitations [13].

A double-walled CN (DWCN) is the simplest form of multi-walled CN. Its physical characteristics are different from those of a SWCN, due to the intertube atomic interactions. These interactions significantly affect the low-energy bands, which are calculated by the tight-binding model [16–19] and the first-principles method [20]. They induce observable changes in the band-edge state, curvature of the energy band, hybridization of wavefunctions, energy spacing between two subbands, and symmetry of the energy spectrum about the Fermi level [16, 17, 20]. The symmetric configurations of the outer and inner tubes also play an important role in the electronic properties. The effects due to different symmetries are directly reflected in the optical absorption spectra [17, 18] and the Coulomb excitations [19].

A magnetic field could modulate the electronic properties of CNs, which are either metallic or semiconducting. For SWCNs or DWCNs, the magnetic field will alter the energy gap, break state degeneracy, and change energy dispersions [17, 21–25]. Moreover, finite SWCNs exhibit special magnetic properties, and their optical spectra are deeply influenced by the magnetic field [12–14]. Besides,

 

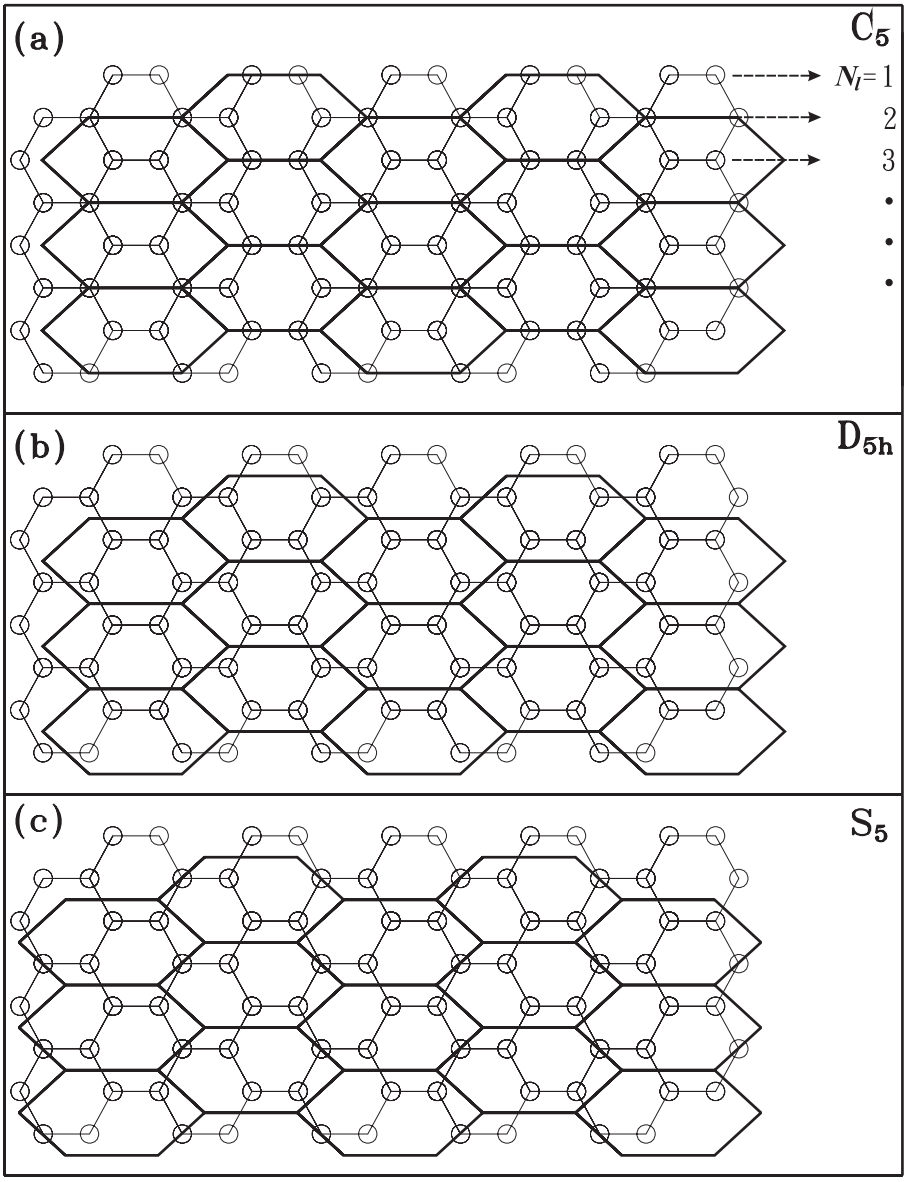


**Figure 1.** The extended geometric structures of coaxial (5, 5)–(10, 10) finite armchair carbon nanotubes are shown in (a) $C_5$, (b) $D_{5h}$, and (c) $S_5$. The inner tube (heavy curves) is projected onto the outer one. $N_l$ is the number of dimer lines along the axial direction.

the essential magnetic property, or the Aharonov–Bohm (AB) effect associated with the magnetic field parallel to the tube axis, has been observed through the transport [26–28] and optical [29, 30] experiments. In this work, electronic structures of finite armchair DWCNs in a uniform magnetic field are studied by the Peierls tight-binding model. Their dependence on the strength and direction of the magnetic field, the tube length, the symmetric configurations, and the Zeeman effect is investigated. The predicted electronic properties could be tested by experimental measurements.

## 2. Theory

The coaxial (5, 5)–(10, 10) finite armchair DWCN was chosen as a model study. Its radius and chirality are uniquely characterized by $m$ and $n$ in a $(m, n)$ SWCN (the detailed geometric structures are given in in [12]). The $C_5$, $D_{5h}$, and $S_5$ symmetric systems are presented in figures 1(a), (b), and (c), respectively. The tube length $L = (N_l - 1)\sqrt{3}b/2$ is proportional to the number of dimer lines $N_l$. $b = 1.42$ Å is the C–C bond length. The inner and outer tubes have the same length, and the total number of atoms in the finite (5, 5)–(10, 10) DWCN is $N_t = 30N_l$. For the $C_5$ system, all the carbon atoms on the inner tube (the heavy line) are projected onto half of those on the outer tube (the light line). The two tubes have the same $z$ coordinates along the symmetry axis. The $C_5$ system becomes a $D_{5h}$ system when the inner tube is axially displaced by $\sqrt{3}b/4$. The $z$ coordinates are different for the inner and outer tubes of the $D_{5h}$ system. An axial clockwise rotation of the inner tube, with an angle of 6°, will further make the $D_{5h}$ system change into a $S_5$ system. Both $D_{5h}$ and $S_5$ systems own the same $z$ coordinates (have a similar boundary structure).

The electronic structures of finite armchair DWCNs are obtained by using the tight-binding model with one $2p_z$ orbital per carbon atom. The Hamiltonian built from the $N_t$ atomic wavefunctions is displayed as

$$H_{kl} = \begin{cases} h(\theta_{kl})c_l^\dagger c_k, \\ \qquad \text{for intratube interactions;} \\ -Wh(\theta_{kl})e^{(a-d_{kl})/\delta}c_l^\dagger c_k, \\ \qquad \text{for intertube interactions.} \end{cases} \quad (1)$$

$c_k$ and $c_l^\dagger$ are the annihilation and creation operators on sites $k$ and $l$. The $2p_z$ orbitals perpendicular to the cylindrical surface may not be parallel to each other. Such misorientation would reduce the $\pi$ bonding ($V_{pp\pi} = -2.66$ eV $= \gamma_0$) and induce extra $\sigma$ bonding ($V_{pp\sigma} = 6.38$ eV). It is noted that the $2p_z$ orbitals on a planar graphene sheet only create $\pi$ bonding. The intratube or the intertube atomic interactions include $V_{pp\pi}$ and $V_{pp\sigma}$, and the effective atomic interactions (or the hopping integrals $h(\theta_{kl})$) depend on the angle $\theta_{kl}$ between two radial vectors of the $k$th and $l$th atoms. As to the intratube part, only the nearest-neighbor atomic interactions are taken into account in the tight-binding model. On the other hand, an exponential function $e^{(a-d_{kl})/\delta}$ is added to the intertube part. $d_{kl}$ is the distance between two $2p_z$ orbitals; $a$ is that between the inner and outer tubes, and $\delta$ equals 0.45 Å. The intertube atomic interactions are cut off for $d_{kl}$ is greater than 3.9 Å, and their strength is modified by $W$ to fit the *ab initio* calculations and experimental data [31].

Finite armchair DWCNs exist in a uniform magnetic field

$$\mathbf{B} = B\cos\alpha\hat{z} + B\sin\alpha\hat{r}, \quad (2)$$

where $\alpha$ is the angle between the field direction and the tube axis. The cylindrical coordinates $(r, \Phi, z)$ are taken in the following calculations. The vector potential associated with $\mathbf{B}$ is given by

$$\mathbf{A} = rB\cos\alpha/2\hat{\Phi} + rB\sin\alpha\sin\Phi\hat{z}, \quad (3)$$

which leads to a Peierls phase difference $\Delta G_{kl} = \int_l^k \mathbf{A}\cdot d\mathbf{r}$ between sites $k$ and $l$. By detailed calculations, the Hamiltonian in the presence of $\mathbf{B}$ is

$$H = \sum_{kl} H_{kl} \times e^{i\frac{e}{\hbar}\Delta G_{kl}}, \quad (4)$$

where

$$\Delta G_{k,l} = \frac{r_k r_l}{2}\sin(\Phi_k - \Phi_l)B\cos\alpha + \frac{(z_k - z_l)}{2}(r_k\sin\Phi_k + r_l\sin\Phi_l)B\sin\alpha. \quad (5)$$

$r_k$ is the inner or outer radius, depending on the atomic position. The magnetic flux, which is defined as $\phi = \pi {r_o}^2 B$, will be used to characterize the field strength $B$. $\phi_0 = hc/e$ is the magnetic flux quantum, and $r_o$ is the radius of the outer (10, 10) CN. By diagonalizing the $N_t \times N_t$ Hamiltonian matrix in equation (4), the discrete state energies $E_J^h$ can be obtained. $(h = c, J)$ and $(h = v, J)$, respectively, represent the $J$th unoccupied and occupied states measured from the Fermi level $E_F = 0$.

## 3. Results

State energies of finite armchair DWCNs affected by the magnetic field and the intertube atomic interactions are studied. The quantized discrete states of the $N_l = 18$ system, without the intertube atomic interactions, are symmetric about the Fermi level, as shown in figure 2(a). The occupied and unoccupied states ($E_{J=1}^{c,v} = \pm 0.02\gamma_0$) nearest to $E_F = 0$ come from the inner (5, 5) tube, while the next two states ($E_{J=2}^{c,v} = \pm 0.075\gamma_0$) arise from the outer (10, 10) one. The energy gap is $E_g = E_{J=1}^c - E_{J=1}^v = 0.04\gamma_0$. The $J = 2$ and 1 states can also be distinguished during the variation of the magnetic field. The former, in the presence of a parallel magnetic field ($\alpha = 0°$; solid circles), exhibit periodic oscillations with a period $\phi_0$. However, the latter have a larger period because of the smaller radius. When the magnetic field is perpendicular to the tube axis (open circles), the low-energy states will increase with increasing field strength.

The $C_5$ system, as shown in figure 2(b), is in sharp contrast to the independent one. The intertube atomic interactions lead to an asymmetric energy spectrum about $E_F = 0$, enhancement of the energy gap ($E_g = 0.064\gamma_0$), and obvious energy shifts. The original $J = 1$ and 2 unoccupied states, respectively, change from $E_{J=1}^c = 0.02\gamma_0$ and $E_{J=2}^c = 0.075\gamma_0$ into $E_{J=1}^v = -0.032\gamma_0$ and $E_{J=2}^c = 0.164\gamma_0$. It should be noticed that the interchange of the $J = 1$ unoccupied and occupied states ($c \leftrightarrow v$) is mainly due to the strong hybridization of the inner and outer tight-binding functions. The contribution from the inner tube is almost equal to that from the outer tube. There exists a weaker hybridization for the original $J = 1$ and $J = 2$ occupied states, in which the state energies alter comparatively mildly ($E_{J=1}^v = -0.02\gamma_0 \rightarrow E_{J=1}^c = 0.032\gamma_0$; $E_{J=2}^v = -0.075\gamma_0 \rightarrow E_{J=2}^v = -0.07\gamma_0$). In this case, the contribution of the tight-binding functions almost results from the original tube. The hybridization between low-energy states of the inner and outer tubes occurs only if these states have similar bonding structures in the tight-binding functions [9]. It hardly affects the symmetric distribution of the tight-binding functions.

When a parallel magnetic field is applied, state energies depend on its strength at $\phi > 0.1\phi_0$. The energy gap gradually grows and then declines in the increase of $\phi$. $E_g$ at $\phi < 0.7\phi_0$ is determined by the occupied and unoccupied states of $J = 1$, while it is associated with the $J = 6$ unoccupied state and the $J = 7$ occupied state for $\phi > 0.7\phi_0$. On the other hand, the effects of the perpendicular magnetic field on electronic properties are negligible at $\phi < 0.3\phi_0$. There are more low-energy states approaching the Fermi level as $\phi$ is larger than $0.3\phi_0$. The energy gap remains almost the same at $\phi < 0.7\phi_0$, and it reduces slightly at others. That the $J = 2$ occupied state is closest to $E_F = 0$ at large flux is responsible for the weak reduction in $E_g$. Finally, the hybridization of the inner and outer tight-binding functions is drastically altered by the parallel and perpendicular magnetic fields. For example, at sufficiently large $\phi$, the $J = 1$ occupied state is dominated by the (5, 5) tube, not by the (5, 5) and (10, 10) tubes (the above-mentioned results at $\phi = 0$).

Electronic properties are associated with the geometric configurations. The $D_{5h}$ system differs somewhat from the $C_5$

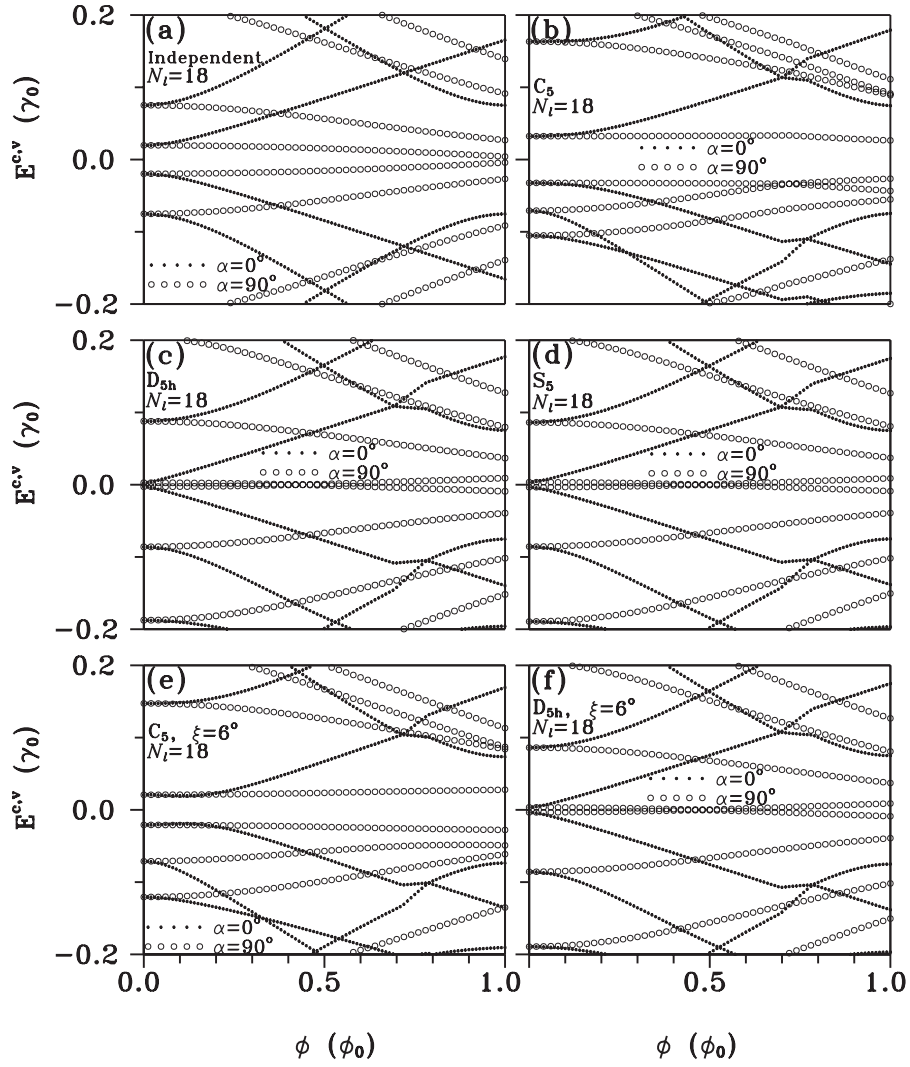


**Figure 2.** The flux-dependent state energies in a parallel or perpendicular magnetic field. They are shown for the (a) independent, (b) $C_5$, (c) $D_{5h}$, (d) $S_5$, (e) ($C_5$, $\xi = 6°$), and (f) ($D_{5h}$, $\xi = 6°$) systems with $N_l = 18$.

system in electronic states and field dependence (figures 2(b) and (c)). Concerning the state energies of $J = 1$, the change due to the intertube atomic interactions in the $D_{5h}$ system ($E^{c,v}_{J=1} = \pm 0.02\gamma_0 \rightarrow E^{c,v}_{J=1} = \pm 0.002\gamma_0$) gets weaker than that in the $C_5$ system and thus forms a smaller energy gap. The atomic hybridization in the former is reduced, since the $2p_z$ orbitals on the inner and outer tubes do not align with each other along the $z$-axis. The dissimilar boundary structures on the two extremities also make the tight-binding functions unsymmetrically distributed in the middle of the finite $D_{5h}$ system. The $J = 1$ state energies strongly depend on the strength of the parallel magnetic field even at $\phi \rightarrow 0$. Although the perpendicular magnetic field has a weaker effect on them, it could make the occupied and unoccupied states of $J = 1$ interchange. Such state crossing is absent in the $C_5$ system. The $S_5$ system shows almost the same electronic state characteristics as the $D_{5h}$ system does (figures 2(c) and (d)). The main reason for this is that these two systems have a similar boundary structure and intertube atomic interactions. Electronic properties are dominated by the boundary structures on the two extremities of a finite DWCN.

The dependence on the rotation angle and the length deserves a closer investigation. The two different terminations, which are obtained by rotating the inner tubes of the $C_5$ and $D_{5h}$ systems counterclockwise about the $z$-axis by an angle $\xi = 6°$, are presented in figures 2(e) and (f), respectively. They do not induce drastic changes in the **B**-field dependence of state energies (figures 2(b) and (e); figures 2(c) and (f)). Moreover, electronic states of the ($D_{5h}$, $\xi = 6°$) are almost the same as those of the $D_{5h}$ and $S_5$ systems (figures 2(f), (c), and (d)). These results further indicate that electronic properties are dominated by the boundary structures along the tube axis, not by the different terminations.

A lot of finite DWCNs, with different lengths, are calculated for their **B**-dependent state energies. To see the length dependence, the $C_5$, $D_{5h}$, and $S_5$ systems of $N_l = 18$ ($N_l = 19$) ($N_l = 20$) are, respectively, shown in figures 2(b)–(d), figures 3(a), (c), (e), and figures 3(b), (d), (f). According to the lengths (I) $N_l = 3i$, (II) $3i + 1$, and (III) $3i + 2$ ($i$ an integer), there are three types of magnetic-field-dependent state energies. The important differences among them lie in

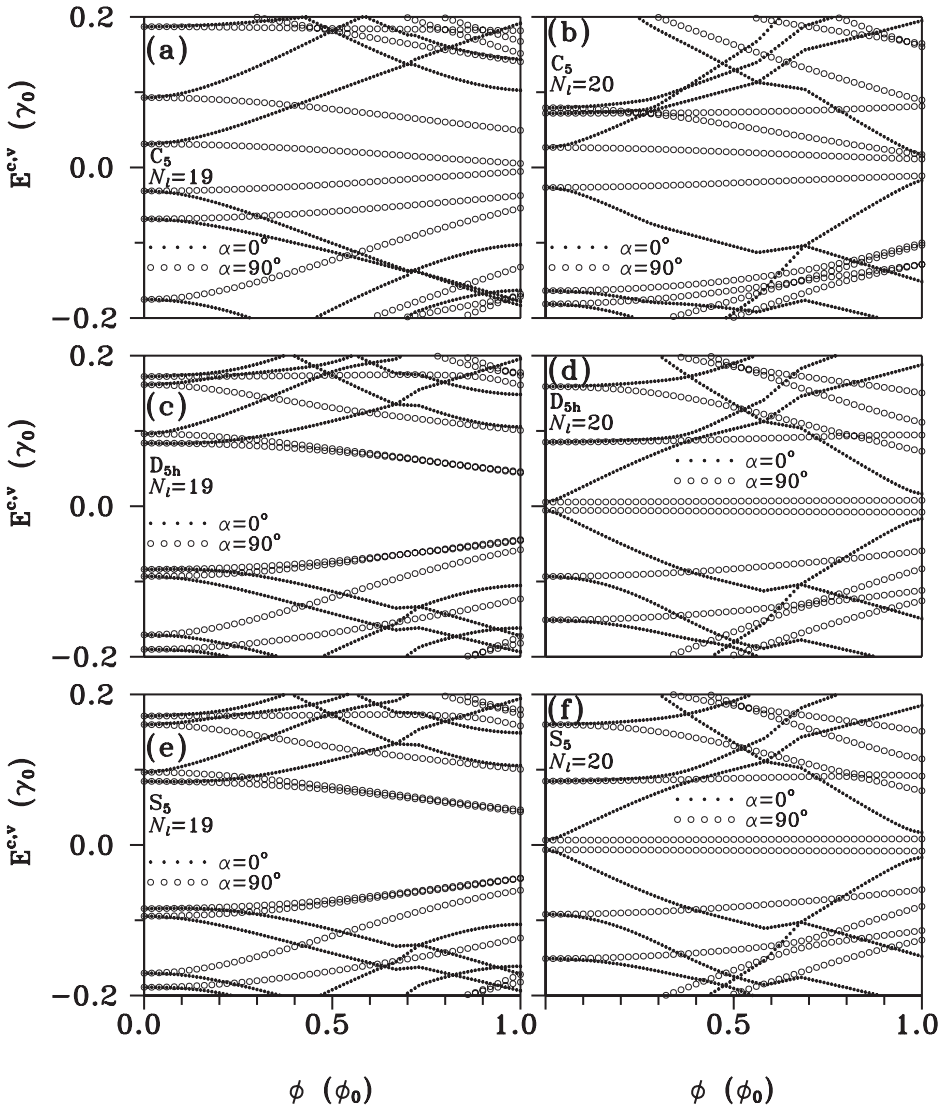


**Figure 3.** Same plots as figure 2, but shown for the (a) ($C_5$, $N_l = 19$), (b) ($C_5$, $N_l = 20$), (c) ($D_{5h}$, $N_l = 19$), (d) ($D_{5h}$, $N_l = 20$), (e) ($S_5$, $N_l = 19$), and (f) ($S_5$, $N_l = 20$) systems.

the energy spacing $E_{s0}$ between the $J = 1$ occupied and unoccupied states at $\alpha = 90°$ and $E^c_{sJ}$ ($E^v_{sJ}$) between the $J$ and $J + 1$ unoccupied (occupied) states. The symmetric $C_5$ configuration is discussed first. $E_{s0}$ of the type-I system grows slowly with increasing of $\phi$ (figure 2(b)), while those of the type-II and type-III systems gradually decrease (figures 3(a) and (b)). Moreover, the values of $E^c_{sJ}$ ($E^v_{sJ}$) greatly contrast with one another. On the other hand, for symmetric $D_{5h}$ ($S_5$) configuration the $\phi$-dependence of $E_{s0}$ can be employed to characterize the three types. When the magnetic flux increases, $E_{s0}$ of the type-I system gradually declines from a finite value to zero and then grows (figures 2(c) and (d)), that of the type-II system decreases rapidly (figures 3(c) and (e)), and that of the type-III system remains almost the same (figures 3(d) and (f)). In addition, the three types will merge into one type as $N_l$ becomes sufficiently large ($N_l > 50$; not shown). The quantum-size effect, the quantization of the electronic states due to the finite length, is expected to vanish when $N_l$ is larger than $10^5$ (average energy spacing $\sim 2\times10^{-6}\gamma_0 = 0.005$ meV).

The main features of the electronic states are directly reflected in the density of states (DOS). The Zeeman splitting is included in the calculations of the DOS. The Zeeman energy is $E_z = g\sigma\phi/m^*r^2\phi_0$, where the $g$ factor is assumed to be the same as that ($\sim$2) of graphite, $\sigma = \pm1/2$ is the electron spin, and $m^*$ is the bare electron mass. The Zeeman effect would lead to a rigid shift for the spin-up and spin-down states, and it could be observed in the DOS. The DOS of a finite DWCN is given by

$$D(\omega,\phi) = \sum_{\sigma,J,h=c,v} \frac{1}{\pi} \frac{\Gamma}{[\omega - E^h_J(\phi,\sigma)]^2 - \Gamma^2}, \qquad (6)$$

where $\Gamma$ ($=10^{-4}\gamma_0$) is the broadening energy width and $E^h_J(\phi,\sigma) = E^h_J(\phi) + E_z$ is the state energy. There are a lot of delta-functional-like prominent peaks in the DOS, mainly owing to the quantized discrete states (figures 4(a)–(d) for $-0.4\gamma_0 \leqslant \omega \leqslant 0.4\gamma_0$). The peak height represents the state degeneracy. The independent system in the absence of **B**, as shown in the inset of figure 4(a),

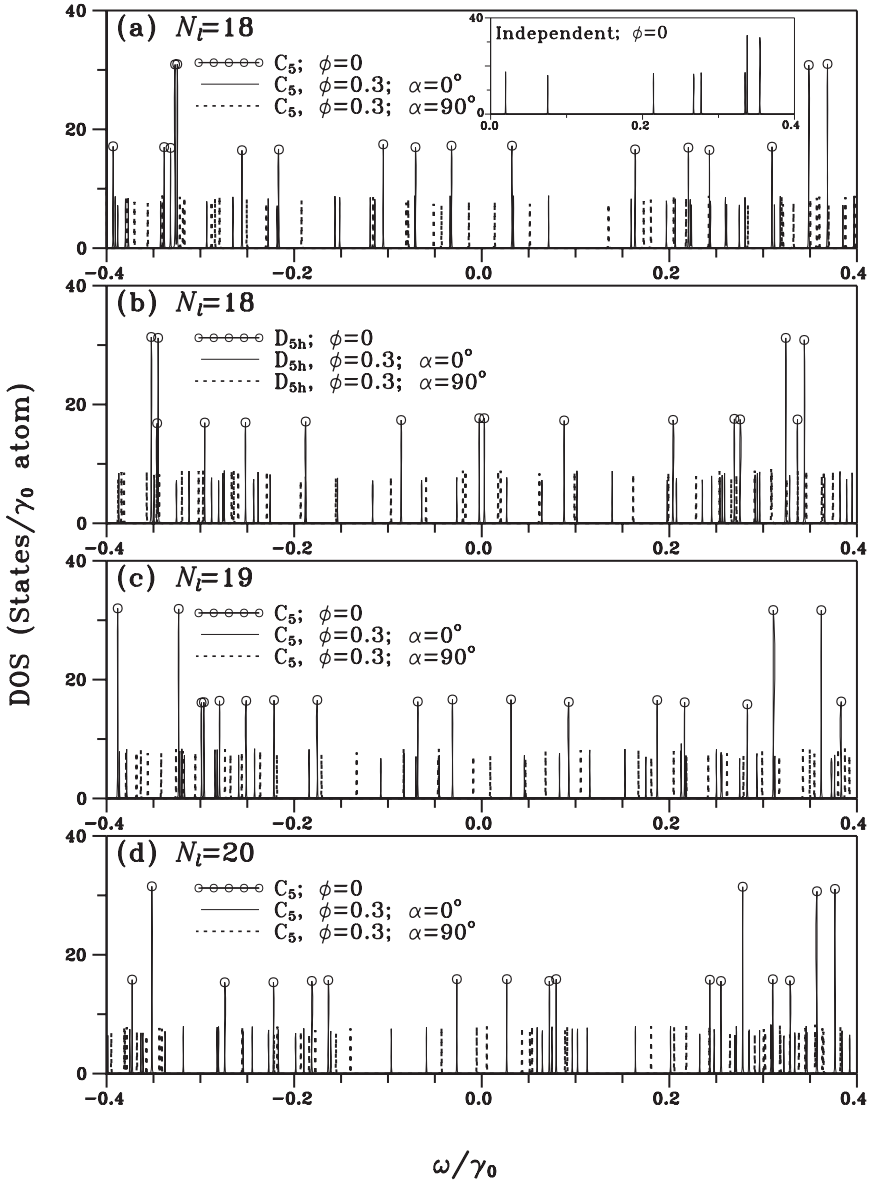


**Figure 4.** Density of states for the (a) $C_5$ and (b) $D_{5h}$ systems of $N_l = 18$ at $\phi = 0$, ($\phi = 0.3\phi_0$, $\alpha = 0°$), and ($\phi = 0.3\phi_0$, $\alpha = 90°$). Similar plots for the $C_5$ systems with (c) $N_l = 19$ and (d) $N_l = 20$. The Zeeman effect is taken into account. The inset in (a) presents that of the independent system at $\phi = 0$.

exhibits the doubly and four-fold degenerate peaks. The intertube atomic interactions in the $C_5$ system drastically change the frequencies and the number of pronounced peaks, and the symmetry of peak structures about $\omega = 0$ (the solid-circled lines in figure 4(a)). They do not affect the peak height or the state degeneracy. The parallel or perpendicular magnetic field lifts the four-fold degeneracy at higher energies resulting in the double degeneracy. The Zeeman effect induces further splitting of the doubly degenerate peaks, so that the DOS only displays the single degenerate peaks (the solid and dashed lines in figure 4(a)). The important difference between $\alpha = 0°$ and 90° in the DOS is the peak frequencies. The effects, due to the intertube atomic interactions and **B**, could also be found in other systems with different boundary structures (figure 4(b)) and lengths (figures 4(c) and (d)). The different geometric structures significantly alter the peak frequency and peak number.

Figure 5(a) presents energy gaps of the $N_l = 18$ $C_5$ system as a function of the magnetic field with different $\alpha$. The dependence of $E_g$ on $\phi$ is strong. For the parallel magnetic field, $E_g$ without the spin-$B$ interaction grows gradually with $\phi$ when $\phi < 0.1\phi_0$, then rises rapidly, and reaches a peak value (the solid line with circles). Finally, it starts to decline at $\phi \sim 0.7\phi_0$. For the case of finite SWCNs, the decrease of $E_g$ first emerges from $\phi = 0.5\phi_0$ (figure 2(a) in [14]). The difference results from the different periods of the inner and outer tubes. The energy gap is significantly reduced by the Zeeman splitting (the heavy solid line). When the magnetic field gradually deviates from the tube axis, $E_g$ is noticeably affected by $\alpha$. At small $\phi$, the energy gap rapidly declines with the increment of $\alpha$. $E_g$ would vanish for a sufficiently

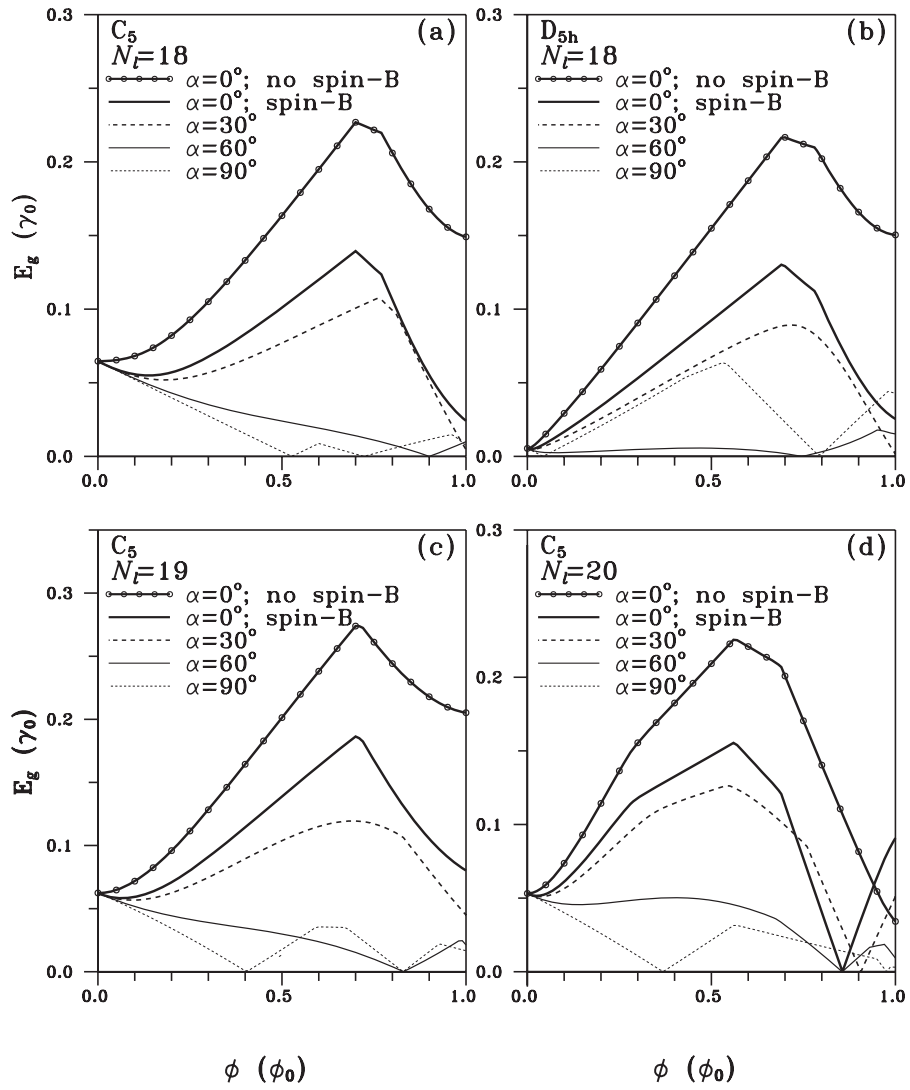


**Figure 5.** The magnetic-flux-dependent energy gaps at different $\alpha$ for (a) the $N_l = 18$ $C_5$ system, (b) the $N_l = 18$ $D_{5h}$ system, (c) the $N_l = 19$ $C_5$ system, and (d) the $N_l = 20$ $C_5$ system. Those without the spin-$B$ interaction at $\alpha = 0°$ are also shown for comparison.

large $\alpha$ ($\alpha \geqslant 45°$). The $\phi$-dependent $E_g$, which changes from a finite value to zero at a certain magnetic flux ($\phi_c$), exhibits a complete energy-gap modulation (CEGM). CEGMs happen more frequently at large $\alpha$, e.g. two occurrences at $\alpha = 90°$ for $\phi \leqslant \phi_0$ (the light dashed line). They are also related to the boundary structure and the length. The first CEGM in the $N_l = 18$ $D_{5h}$ system occurs at a lower $\phi_c$ compared with that in the $N_l = 18$ $C_5$ system (figures 5(b) and (a)). That its energy gap in the absence of **B** is very small could account for this result. The main features of the CEGMs are different for the three types of DWCN, as shown in figures 5(a), (c) and (d) for the $C_5$ systems of $N_l = 18$, 19, and 20, respectively. The important differences include the values of $\phi_c$, the occurrence of CEGM, and dependence on the field direction. It is noticed that the $N_l = 20$ $C_5$ system exhibits CEGM even in the parallel magnetic field (the heavy solid line in figure 5(d)), and $\phi_c$ at $\alpha = 0°$ is smaller than that at $\alpha = 30°$. In short, the energy gap could be effectively modulated by the strength and direction of the magnetic field, the Zeeman splitting, and the geometric structures.

## 4. Conclusions

In conclusion, for finite double-walled armchair CNs we have calculated electronic properties in a magnetic field by using the Peierls tight-binding model. The state energy, wavefunction, energy gap, and density of states are dominated by the intertube atomic interactions, magnitude and direction of the magnetic field, boundary structure, length, and Zeeman splitting. The intertube atomic interactions destroy the symmetric energy spectrum about the Fermi level, alter the energy gap, and cause visible energy shifts. The magnetic field could induce state crossing, drastic changes in the hybridization of the inner and outer tight-binding functions, destruction of state degeneracy, more low-energy states, and CEGMs. CEGMs happen more frequently at large $\alpha$ or $N_l$. The dissimilar boundary structures make the $C_5$ system sharply contrast with the $D_{5h}$ or $S_5$ system in the strength of the intertube atomic hoppings, distribution of the tight-binding functions, and dependence on the magnetic field. According to the lengths $N_l = 3i$, $3i + 1$, and $3i + 2$, state energies exhibit three types of magnetic flux

dependence. Two kinds of boundary structure and three types of length considered in this work are sufficient to illustrate the essential electronic properties of finite DWCNs. The energy gap is significantly reduced by the Zeeman splitting; therefore, CEGMs occur at smaller magnetic fields. The main features of discrete states are directly reflected in the DOS, e.g. the number, frequency, and height of pronounced symmetric peaks. The experimental measurements of electrical conductance [26–28] and the absorption spectrum [29, 30] could be utilized to examine predicted magneto-electronic properties.

## References


[1] Iijima S 1991 *Nature* **354** 56
[2] Venema L C, Wildöer J W G, Tuinstra H L J T, Dekker C, Rinzler A G and Smalley R E 1997 *Appl. Phys. Lett.* **71** 2629
[3] Tans S J, Devoret M H, Dai H, Thess A, Smalley R E, Geerligs L J and Dekker C 1997 *Nature* **386** 474
[4] Venema L C, Wildöer J W G, Janssen J W, Tans S J, Hinne L J, Tuinstra T, Kouwenhoven L P and Dekker C 1999 *Science* **283** 52
[5] Nygård J, Cobden D H and Lindelof P E 2000 *Nature* **408** 342
[6] Cobden D H and Nygård J 2002 *Phys. Rev. Lett.* **89** 046803
[7] Jarillo-Herrero P, Sapmaz S, Dekker C, Kouwenhoven L P and Van der Zant H S J 2004 *Nature* **429** 389
[8] Moriyama S, Fuse T, Suzuki M, Aoyagi Y and Ishibashi K 2005 *Phys. Rev. Lett.* **94** 186806
[9] Rubio A, Sánchez-Portal D, Artacho E, Ordeján P and Soler J M 1999 *Phys. Rev. Lett.* **82** 3520
[10] Jishi R A, Bragin J and Lou L 1999 *Phys. Rev.* B **59** 9862
[11] Matsuo Y, Tahara K and Nakamura E 2003 *Org. Lett.* **5** 3181
[12] Chen R B, Lu B J, Tsai C C, Chang C P, Shyu F L and Lin M F 2004 *Carbon* **42** 2873
[13] Chen R B, Chang C P, Shyu F L, Hwang J S and Lin M F 2004 *Carbon* **42** 531
[14] Chen R B, Chang C P, Hwang J S, Chuu D S and Lin M F 2005 *J. Phys. Soc. Japan* **74** 1404
[15] Lee C H, Chen R B, Li T S, Chang C P and Lin M F 2006 *J. Phys.: Condens. Matter* **18** 9427
[16] Saito R, Dresselhaus G and Dresselhaus M S 1993 *J. Appl. Phys.* **73** 494
[17] Ho Y H, Chang C P, Shyu F L, Chen R B, Chne S C and Lin M F 2004 *Carbon* **42** 3159
[18] Ho G W, Ho Y H, Li T S, Chang C P and Lin M F 2006 *Carbon* **44** 2323
[19] Ho Y H, Ho G W, Chen S C, Ho J H and Lin M F 2007 *Phys. Rev.* B **76** 115422
[20] Kwon Y K and Tománek D 1998 *Phys. Rev.* B **58** R16001
[21] Ajiki H and Ando T 1993 *J. Phys. Soc. Japan* **62** 1255
[22] Ajiki H and Ando T 1993 *J. Phys. Soc. Japan* **62** 2470
[23] Ajiki H and Ando T 1995 *J. Phys. Soc. Japan* **64** 4382
[24] Lin M F and Shung K W K 1995 *Phys. Rev.* B **52** 8423
[25] Shyu F L, Chang C P, Chen R B, Chiu C W and Lin M F 2003 *Phys. Rev.* B **67** 045405
[26] Stojetz B, Miko C, Forró L and Strunk C 2005 *Phys. Rev. Lett.* **94** 186802
[27] Strunk C, Stojetz B and Roche S 2006 *Semicond. Sci. Technol.* **21** S38
[28] Stojetz B, Roche S, Triozon F, Forró L and Strunk C 2007 *New J. Phys.* **9** 56
[29] Zaric S *et al* 2004 *Science* **304** 1129
[30] Mortimer I B, Li L-J, Taylor R A, Rikken G L, Portugall J A and Nicholas R J 2003 *Phys. Rev.* B **76** 085404
[31] Ahn K-H, Kim Y-H, Wiersig J and Chang K J 2003 *Phys. Rev. Lett.* **90** 026601